Vessel co-option mediates resistance to anti-angiogenic therapy in liver metastases

Sophia Frentzas[#1,2], **Eve Simoneau**[#3], **Victoria L. Bridgeman**[#1], **Peter B. Vermeulen**[#1,4], **Shane Foo**[1], **Eleftherios Kostaras**[1], **Mark Nathan**[1], **Andrew Wotherspoon**[2], **Zu-hua Gao**[3], **Yu Shi**[3], **Gert Van den Eynden**[4], **Frances Daley**[5], **Clare Peckitt**[2], **Xianming Tan**[6], **Ayat Salman**[3], **Anthoula Lazaris**[3], **Patrycja Gazinska**[7], **Tracy J. Berg**[1], **Zak Eltahir**[2], **Laila Ritsma**[8], **Jacco Van Rheenen**[8], **Alla Khashper**[3], **Gina Brown**[2], **Hanna Nystrom**[9], **Malin Sund**[9], **Steven Van Laere**[4], **Evelyne Loyer**[10], **Luc Dirix**[4], **David Cunningham**[2,12], **Peter Metrakos**[3,12], and **Andrew R. Reynolds**[1,12]

[1]Tumour Biology Team, The Breast Cancer Now Toby Robins Research Centre, The Institute of Cancer Research, London, UK [2]The Royal Marsden, London, UK [3]McGill University Health Centre, Royal Victoria Hospital - Glen Site, Montreal, Quebec, Canada [4]Translational Cancer Research Unit, Gasthuis Zusters Antwerpen Hospitals St. Augustinus, Antwerp, Belgium [5]Breast Cancer Now Histopathology Core Facility, The Royal Marsden, London, UK [6]Lineberger Comprehensive Cancer Center, University of North Carolina, Chapel Hill, NC, USA [7]Breast Cancer Now Unit, Guy's Hospital, King's College London School of Medicine, London, UK [8]Cancer Genomics Center-Hubrecht Institute-Royal Netherlands Academy of Arts and Sciences & University Medical Centre Utrecht, Uppsalalaan 8, Utrecht 3584CT, Netherlands [9]Department of Surgical and Perioperative Sciences, Umeå University, Umea, Sweden [10]The University of Texas MD Anderson Cancer Center, Houston, TX, USA

[#] These authors contributed equally to this work.

Abstract

The efficacy of angiogenesis inhibitors in cancer is limited by resistance mechanisms that are poorly understood. Notably, instead of inducing angiogenesis, some cancers vascularize by the

non-angiogenic mechanism of vessel co-option. Here we show that vessel co-option is associated with a poor response to the anti-angiogenic agent bevacizumab in patients with colorectal cancer liver metastases. Moreover, we find that vessel co-option prevails in human breast cancer liver metastases, a setting where results with anti-angiogenic therapy have been disappointing. In our preclinical mechanistic studies, we show that cancer cell motility mediated by the Arp2/3 complex is required for vessel co-option in liver metastases *in vivo* and that combined inhibition of angiogenesis and vessel co-option is more effective than inhibiting angiogenesis alone in this setting. Vessel co-option is therefore a clinically relevant mechanism of resistance to anti-angiogenic therapy and combined inhibition of angiogenesis and vessel co-option may be a warranted therapeutic strategy.

Introduction

Metastases can vascularize through sprouting angiogenesis that is stimulated by vascular endothelial growth factor-A (VEGF-A). This prompted the clinical development of anti-angiogenic agents, including the VEGF-A targeted antibody, bevacizumab[1,2]. Bevacizumab combined with chemotherapy (bev-chemo) can extend progression-free and / or overall survival in several indications, including metastatic colorectal cancer (CRC)[3,4]. Indeed, bev-chemo is now an approved treatment for many different cancer types, including metastatic CRC. Despite this fact, the survival benefit achieved with the addition of bevacizumab to chemotherapy is modest, measured only in terms of months. Moreover, in other indications, including metastatic breast cancer, anti-angiogenic therapy has yet to demonstrate a survival benefit in patients[5,6]. The mechanisms that limit the therapeutic efficacy of anti-angiogenic therapy in patients are still poorly understood.

However, it now emerges that some metastases can also vascularize by the non-angiogenic mechanism of vessel co-option, a process whereby cancer cells incorporate pre-existing vessels from surrounding tissue instead of inducing new vessel growth[7–10]. Notably, although anti-angiogenic agents (including bevacizumab) were designed to target sprouting angiogenesis, they were not designed to target the process of vessel co-option. Because of this, vessel co-option has been suggested as a potential mechanism of resistance to anti-angiogenic therapy[6,10,11]. In the current study, we provide the first evidence that vessel co-option is a clinically relevant mechanism of resistance to anti-angiogenic therapy in liver metastases and that combined inhibition of angiogenesis and vessel co-option is more effective than targeting angiogenesis alone.

Results

Replacement growth pattern liver metastases respond poorly to bevacizumab

The liver is the most common site of involvement in metastatic CRC, and surgical removal of CRC liver metastases (CRCLMs) is now recommended practice for eligible patients[12]. Careful histopathological examination of human CRCLMs has shown that these tumors can present with three different histopathological growth patterns (HGPs): the desmoplastic HGP, the pushing HGP or the replacement HGP (Fig. 1a and Supplementary Fig. 1)[8,13]. These growth patterns have distinct histopathological features and utilise different

mechanisms to obtain a vascular supply. In the desmoplastic HGP, the cancer cells are seperated from the normal liver parenchyma by a capsule of desmoplastic stroma. In the pushing HGP, there is no desmoplastic capsule but the cancer cells push the normal liver parenchyma away. Both of these growth patterns utilise angiogenesis to obtain a vascular supply. However, in metastases with a replacement HGP, the cancer cells infiltrate the liver parenchyma and co-opt pre-existing sinusoidal vessels instead of promoting angiogenesis[8,13,14]. Although bevacizumab was not designed to target vessel co-option, no study has addressed whether the replacement growth pattern (where vessel co-option occurs) is associated with resistance to bevacizumab in liver metastases.

To address this question, we took advantage of the fact that some patients with metastatic CRC receive preoperative therapy with bev-chemo in the months that precede surgical removal of CRCLMs[15–17]. We evaluated the HGPs and the pathological response to therapy in 59 CRCLMs resected from 33 patients that were treated preoperatively with bev-chemo at The Royal Marsden (RM) by examining haematoxylin and eosin (H&E) stained liver resection specimens (Fig. 1b) (for patient details see Supplementary Fig. 2 and Supplementary Table 1). Since CRCLMs can present with a mixture of HGPs[13], the percentage of desmoplastic, pushing and replacement HGP was quantified in each lesion. To measure response to therapy, the pathological response in each lesion was scored in quartiles (>75%, 50–75%, 25–49% or <25% viable tumor). Lesions with <25% viable tumor were considered good responders, whilst lesions with 25% viable tumor were considered poor responders.

Notably, lesions having a substantial (50%) replacement component were significantly enriched in the group of lesions classified as poor responders when compared to the group of lesions classified as good responders (Fig. 1b, $P<0.001$). In contrast, lesions having a substantial (50%) desmoplastic component were significantly enriched in the group of lesions classified as good responders when compared to the group of lesions classified as poor responders (Fig. 1b, $P<0.001$). Similar results were obtained when the same analysis was repeated using only the single largest lesion from each patient (Supplementary Fig. 3). In a univariate analysis of other clinical variables, only the HGP showed a statistically significant association with pathological response (Supplementary Table 2).

Some examples of the lesions examined for this analysis are shown in Fig. 1c–e. In Fig. 1c, a lesion scored as >75% viable with HGP score of 100% replacement is shown. Note the close contact between tumor cells and liver parenchyma in the infiltrative replacement growth pattern (arrows). In Fig. 1d, a lesion scored as <25% viable with HGP score of 100% desmoplastic is shown. Note the entire circumference of the tumor is desmoplastic and well encapsulated (arrowheads). A large central area of infarct-like necrosis (ILN), indicative of a strong treatment response, is labeled (asterisks). In Fig. 1e, a lesion scored as >25% viable that has a mixed growth pattern (79% desmoplastic, 19% replacement, 2% pushing) is shown. Note the presence of a desmoplastic rim at the periphery of the tumour (arrowheads) which surrounds a large central area of ILN (asterisks). However, at the periphery of the tumour, two viable nodules with a replacement HGP can be seen (arrows).

To validate the association between the HGPs and pathological response to therapy, we then examined a larger series of 128 CRCLMs from 59 patients that were treated preoperatively with bev-chemo at McGill University Health Centre (MUHC) (for patient details see Supplementary Fig. 4 and Supplementary Table 3). Again, lesions with 50% replacement HGP were significantly enriched in the poorly responding group of lesions (Fig. 1f, P >0.001), whilst lesions with 50% desmoplastic HGP were significantly enriched in the group of lesions classified as good responders (Fig. 1f, P>0.001). Similar results were obtained when the same analysis was repeated using only the single largest lesion from each patient (Supplementary Fig. 5). In a univariate analysis, the HGP was the strongest predictor of pathological response (Supplementary Table 4).

Included in these analyses were both patients that presented with a solitary liver metastasis and patients that presented with multiple liver metastases. To control for this, we also examined the subset of patients that presented with a single lesion only (pooled from RM and MUHC). The HGP also correlated with pathological response in this subset of patients (Supplementary Fig. 6). A univariate and multivariate analyses of 181 lesions from 90 patients (pooled from RM and MUHC) was also performed to determine clinical characteristics associated with a good pathological response (Supplementary Table 5). Only the HGPs showed a statistically significant association with pathological response. The replacement HGP was associated with a lower probability of obtaining a good pathological response (OR=0.07, 95% CI 0.03–0.16, P<0.0001 in univariate and OR=0.06, 95% CI 0.03–0.15, P<0.0001 in multivariate). In contrast, the desmoplastic HGP was associated with a higher probability of obtaining a good pathological response (OR=15.06, 95% CI 6.32–35.87, P<0.0001 in univariate and OR=15.92, 95% CI 6.76–37.51, P<0.0001 in multivariate). Taken together, these data demonstrate that the replacement HGP is associated with a poor pathological response to bev-chemo in CRCLMs.

To provide an alternative measure of treatment response, we also evaluated radiological response in the cohort of lesions from the RM patients. Recently published guidelines recommend that response to bev-chemo should be evaluated from computed tomography (CT) scans using novel morphological response criteria which correlate better with outcome than RECIST-based criteria[12,18,19]. Lesions with 50% replacement HGP were significantly enriched in the poor response group according to morphological response criteria (Fig. 2; P=0.006). Similar results were obtained when the same analysis was repeated using only the single largest lesion from each patient (Supplementary Fig. 7). These data provide independent verification that CRCLMs with a replacement HGP respond poorly to bevacizumab. However, notably, no correlation between the HGP and response to therapy was observed when using RECIST-based criteria as a measure of response (Supplementary Fig. 8).

Cancer cells infiltrate the hepatic plates and co-opt sinusoidal blood vessels in the replacement growth pattern

We then investigated the mechanism of tumor vascularization in replacement HGP CRCLMs by examining, in detail, the relationship between cancer cells and the normal liver in this growth pattern. In normal liver, staining for hepatocyte specific antigen (HSA) identified

hepatocytes within the hepatic plates, whilst collagen-3 staining identified the intervening sinusoidal blood vessels (SV; Fig. 3a). In the replacement HGP, co-staining for cancer cells (pan-cytokeratin) and hepatocytes (HSA) demonstrated that invading cancer cells line-up neatly with hepatocytes within the hepatic plates at the tumor-liver interface (Fig. 3b). Replacement of hepatocytes by invading cancer cells was clearly observed (Fig. 3c). Behind the invasive tumor front, near complete replacement of hepatocytes by cancer cells was evident and flattened displaced hepatocytes were frequently observed at the edge of cancer cell nests (Fig. 3d). However, cancer cells clearly respected the spaces occupied by SV (Fig. 3b–d). Therefore, in the replacement growth pattern of liver metastasis, cancer cells (a) invade the liver parenchyma, (b) replace hepatocytes and (c) co-opt SV.

Further evidence for vessel co-option was obtained by staining for the endothelial marker CD31. In the replacement HGP, SV were frequently observed where one end of the vessel was physically located in the normal liver (arrows in Fig. 3e–g), whilst the other end was embedded in the tumor (arrowheads in Fig. 3e–g), showing that these tumors co-opt SV as they infiltrate the liver parenchyma (see also Supplementary Fig. 9a,b). However, this was not observed in the desmoplastic or pushing HGPs (Supplementary Fig. 9c–f). In addition, co-staining of tumors for CD31 and HSA demonstrated that tumor vessels at the periphery of replacement HGP metastases were often still physically associated with hepatocytes, providing additional evidence that these vessels are co-opted sinusoidal vessels and that they are not newly formed vessels (Supplementary Fig. 10a,b). However, this was not observed in the desmoplastic or pushing HGPs (Supplementary Fig. 10c,d). Therefore, whilst replacement HGP CRCLMs co-opt pre-existing sinusoidal vessels, the desmoplastic and pushing CRCLMs do not.

Prevalence of the replacement growth pattern in disease that progresses following bevacizumab treatment

Unfortunately, patients can progress following treatment with bev-chemo by developing new CRCLMs20. Here we define new CRCLMs as lesions that presented in the liver after the initiation of bev-chemo treatment that were not evident on pre-treatment scans. In our analyses of treatment response described above (Fig. 1) we only examined resected CRCLMs that were detected on pre-treatment scans prior to treatment initiation and we specifically excluded any new CRCLMs, even if they were resected. Given that these new CRCLMs represent progressive disease that is clearly resistant to bev-chemo, we identified these new CRCLMs and examined their HGP. In the MUHC case series, 35 new CRCLMs from 13 patients were available for assessment (for patient details see Supplementary Table 6). We compared the HGPs in these new CRCLMs with two control groups from MUHC: pre-existing CRCLMs, i.e. lesions that were resected from bev-chemo treated patients that were detected on pre-treatment scans prior to treatment initiation (128 CRCLMs from 59 patients; for patient details see Supplementary Table 3) and untreated CRCLMs, i.e. lesions resected from MUHC patients that did not receive any pre-operative therapy (32 CRCLMs from 19 patients; for patient details see Supplementary Table 7). The percentage of tumor scored as having a replacement HGP was significantly increased in new CRCLMs compared to the CRCLMs in both control groups ($P<0.001$, Fig. 4a). This was mirrored by a concomitant significant decrease in the desmoplastic HGP in new CRCLMs compared to

both control groups (*P*<0.001, Fig. 4a). These data provide evidence for an increased prevalence of the replacement HGP in patients that progress following treatment with bev-chemo.

Patients with replacement growth pattern liver metastases achieve less clinical benefit from bevacizumab

We then examined whether the HGPs of liver metastasis could impact on the clinical benefit achieved with anti-angiogenic therapy in terms of patient survival (Fig. 4b-f). Kaplan-Meier estimates of overall survival (OS) were calculated for a cohort of 62 patients from MUHC that were treated preoperatively with bev-chemo between 2008 and 2014 and for a cohort of 29 patients from MUHC that were treated preoperatively with chemotherapy alone during the same period. Patients were stratified into groups based on their liver metastasis growth pattern: predominant replacement HGP, predominant desmoplastic HGP or predominant pushing HGP (see Online Methods for details of how these groups were defined).

In the bev-chemo cohort, the predominant desmoplastic HGP patients had a significantly better OS when compared to the predominant replacement HGP patients (HR=3.50, 95%CI 1.49–8.20, *P*=0.0022; Fig. 4b). These data suggest that patients with replacement HGP liver metastases achieve less clinical benefit from treatment with bevacizumab than patients with desmoplastic HGP liver metastases. The HGP was the only variable that showed a statistically significant association with OS in univariate and multivariate analyses (Supplementary Table 8). In addition, both 3-year and 5-year OS were longer for desmoplastic HGP patients compared to replacement HGP patients in the bev-chemo cohort (Fig. 4f). However, in the cohort treated with chemotherapy only, no significant difference in OS was observed between the desmoplastic HGP and replacement HGP patients (HR=0.90, 95%CI 0.31–2.61, *P*=0.846; Fig. 4c).

Additional analyses were also performed as follows. Using the same data set, we examined for a difference in OS between desmoplastic HGP patients that received chemotherapy alone and desmoplastic HGP patients that received bev-chemo. The difference in OS was not statistically significant (HR=2.49, 95%CI 0.93–6.67, *P*=0.0605; Fig. 4d). We also examined for a difference in OS between replacement HGP patients that received chemotherapy alone and replacement HGP patients that received bev-chemo. Again, the difference in OS was not significant (HR=0.69, 95%CI 0.27–1.77, *P*=0.433; Fig. 4e). A comparison of the replacement group with the desmoplastic group showed that the patients were similar in terms of their clinical characteristics (Supplementary Table 9). However, the interval between last dose of therapy and resection tended to be longer in the replacement group compared to the desmoplastic group (median of 83 days interval for replacement patients versus 62 days for desmoplastic patients, *P*=0.030). We also examined for differences in clinical characteristics between the bev-chemo treated cohort and the cohort treated with chemotherapy alone (Supplementary Table 10). The cohorts were similar except for a larger proportion of patients receiving irinotecan-based chemotherapy in the bev-chemo cohort compared to the chemotherapy alone cohort (19% of bev-chemo patients received irinotecan versus 10.3% of chemotherapy alone patients, *P*=0.019).

When stratifying patients based on their liver metastasis HGPs, only two patients were designated in the predominant pushing group (one patient treated with bev-chemo and one patient treated with chemotherapy alone). Due to this fact, these patients were not included in the Kaplan-Meier analysis. However, both of these patients had a poor outcome because they died within 2 years of diagnosis of liver metastasis. This is consistent with the findings of a previous study, which showed that the pushing HGP is an independent predictor of poor overall survival at 2 years of follow-up[21]. It is therefore possible that the pushing HGP of CRCLMs is associated with a poor outcome regardless of the treatment modality utilized.

The replacement HGP is prevalent in breast cancer liver metastases

Thus far, disappointing results have been obtained with anti-angiogenic therapy in metastatic breast cancer[5,6]. Therefore, we also examined the HGPs in breast cancer liver metastasis samples, obtained from 17 patients, by examining H&E-stained tissue sections (for patient details see Supplementary Table 11). The replacement HGP was predominant in 16 of 17 cases examined, with only one case presenting with a predominant desmoplastic HGP (Fig. 5a). Further histopathological characterization of replacement HGP BCLMs is presented in Fig. 5b–g. Breast cancer cells colonized the liver by replacing resident hepatocytes (Fig. 5d) with no desmoplastic stroma present at the tumor-liver interface (Fig. 5e). The vascular architecture of the adjacent liver was preserved at the tumor-liver interface (Fig. 5f) and the co-option of sinusoidal vessels was observed (Fig. 5g). These data show that the replacement HGP, which vascularizes by vessel co-option, predominates in breast cancer liver metastases.

Combined inhibition of vessel co-option and angiogenesis is more effective than inhibition of angiogenesis alone

Vessel co-option in the liver requires the infiltration of cancer cells into the normal liver parenchyma (for example see Fig. 3). We therefore reasoned that cancer cell motility may be required for vessel co-option. The Actin Related Proteins 2/3 complex (Arp2/3 complex) mediates the nucleation of actin filaments at the leading edge of cells to drive cell movement, and has been previously implicated in the motility and invasion of both breast cancer cells and colorectal cancer cells[22–24]. In order to confirm expression of the Arp2/3 complex in human liver metastases, we performed staining for the Arp2/3 subunit ARPC3 using a well-validated antibody. ARPC3 was expressed in cancer cells in all human specimens we examined. Moreover, ARPC3 expression was significantly higher in replacement HGP metastases when compared to desmoplastic HGP metastases (Supplementary Fig. 11).

To then address whether cancer cell motility mediated by Arp2/3 could play a functional role in the process of vessel co-option *in vivo*, we utilized a preclinical orthotopic model of advanced liver metastasis where HT29 colorectal cancer cells are directly injected into mouse liver (Supplementary Fig. 12). This model is commonly used to replicate the advanced stage of CRCLMs where patients are treated in the metastatic setting[25–27]. The CRCLMs generated in this model had a mixed HGP, being mainly composed of replacement HGP areas (Fig. 6a) and, to a lesser extent, desmoplastic HGP areas (Fig. 6b), thus recapitulating the two prevalent HGPs observed in human CRCLMs. We then attempted to knock-down ARPC3 expression in HT29 cells using three different ARPC3-targeting

shRNA oligonucleotides. Two of these oligonucleotides (shARPC3-2 and shARPC3-3) significantly reduced ARPC3 expression in cells, whereas the third oligonucleotide (shARPC3-1), and a control non-targeting oligonucleotide (control shRNA), did not reduce ARPC3 expression in cells (Fig. 6c). In addition, knockdown of ARPC3 significantly suppressed the migration of HT29 cells (Fig. 6d) without any confounding effect on cell proliferation (Supplementary Fig. 13). Notably, knockdown of ARPC3 significantly decreased the replacement HGP *in vivo*, whilst significantly increasing the desmoplastic HGP (Fig. 6e). These data confirm that suppression of Arp2/3-mediated cancer cell motility inhibits the replacement HGP within this *in vivo* model and therefore also blocks the ability of these tumors to co-opt pre-existing liver vessels *in vivo.*

We then evaluated whether combined inhibition of vessel co-option and angiogenesis is more effective at limiting tumor growth when compared to angiogenesis inhibition alone. Mice with established control- or ARPC3-knockdown tumors were treated with the VEGF-A inhibitory antibody B20-4.1.128 combined with capecitabine (Fig. 6f–h). In control tumors, which have a predominantly replacement HGP (Fig. 6f), no significant inhibition of tumor burden was observed in response to treatment when compared to vehicle control (Fig. 6g). However, in ARPC3 knockdown tumors, which have a predominantly desmoplastic HGP (Fig. 6f), tumor burden was significantly suppressed by treatment (Fig. 6g). In addition, although treatment with B20-4.1.1 led to a reduced tumor vessel density in both control- and ARPC3 knockdown-tumors, this effect was more pronounced when vessel co-option was suppressed by knockdown of ARPC3 (Fig. 6h, Supplementary Fig. 14). The administration of capecitabine alone did not significantly suppress tumor burden or tumor vessel density in either control- or ARPC3-knockdown tumors (Supplementary Fig. 15). These data suggest that simultaneous inhibition of angiogenesis and vessel co-option may be a more effective strategy for the treatment of advanced liver metastases than current strategies which target angiogenesis alone.

Discussion

When cancers metastasize to highly vascular organs (including the liver) they can sometimes utilize vessel co-option, instead of angiogenesis, as a mechanism to obtain a vascular supply10. Here we addressed whether vessel co-option could be a significant mechanism of resistance to anti-angiogenic therapy in patients with colorectal cancer liver metastases. We found that: (a) vessel co-option was the predominant mechanism of vascularization in approximately 40% of the lesions we examined, (b) metastases that utilized vessel co-option responded poorly to bev-chemo, (c) vessel co-option was prevalent in patients that progressed following treatment with bev-chemo, and (d) patients with metastases that utilized vessel co-option obtained less clinical benefit from bev-chemo in terms of overall survival. These observations strongly suggest that vessel co-option can blunt the therapeutic benefit achieved with anti-angiogenic therapy in metastatic colorectal cancer.

Our findings also have relevance for breast cancer. Phase 3 trials of bevacizumab combined with chemotherapy in metastatic breast cancer have consistently failed to demonstrate a survival benefit for the addition of bevacizumab29–33. Here we found that the majority of breast cancer liver metastases utilize vessel co-option. In addition, vessel co-option occurs in

breast cancer metastases to the lymph nodes34,35, skin36, lungs7,37,38 and brain39–41. The prevalence of vessel co-option in breast cancer may explain, at least in part, why anti-angiogenic therapy has been a disappointing therapeutic approach in metastatic breast cancer.

Biomarkers that are predictive of response to anti-angiogenic therapy in patients remain elusive6,11,42. Our data suggest that patients who present with desmoplastic HGP liver metastases may derive more benefit from bevacizumab than patients who present with replacement HGP liver metastases, which identifies the HGPs as potential biomarkers for anti-angiogenic therapy. There are some characteristics that are present on magnetic resonance imaging (MRI) of the liver, or CT imaging of the liver, that might be exploited to determine the HGPs of liver metastases prior to treatment. By using imaging to identify liver metastasis HGPs in this way, it may eventually be possible to select-out the patients with desmoplastic HGP liver metastases who are more likely to benefit from anti-angiogenic therapy.

However, in the longer term, we believe that therapeutic strategies which can block vessel co-option in tumors should also be developed. In this regard, here we show that knockdown of Arp2/3-mediated cancer cell motility suppresses vessel co-option in a preclinical model of advanced liver metastasis. Moreover, Kuczynski *et al* recently showed that acquired resistance to the anti-angiogenic drug sorafenib in hepatocellular carcinoma occurs due to increased cancer cell invasion in the liver which mediates co-option of pre-existing liver vessels43. Taken together, these and other data44–51, suggest a key role for cancer cell motility and cancer cell invasion in the process of vessel co-option and that targeting cancer cell movement might, therefore, be an effective means to block vessel co-option in tumors.

In the current manuscript, we also present preclinical evidence that combined inhibition of angiogenesis and vessel co-option is more effective at controlling tumor burden than targeting angiogenesis alone. We propose therefore that therapies which are designed to inhibit both angiogenesis and vessel co-option should be explored in patients, as these may yield greater therapeutic benefit than current therapies that are designed to target angiogenesis alone.

Online Methods

Human samples

Specimens were obtained from patients treated at The Royal Marsden (RM) in London, at McGill University Health Centre (MUHC) in Montreal and at Gasthuis Zusters Antwerpen (GZA) Hospitals St Augustinus in Antwerp. Informed consent was obtained from all patients. Ethical approval was granted by the local Research Ethics Committee at The Royal Marsden, the McGill University Health Centre Research Ethics Board and by the local Research Ethics Committee of the GZA Hospitals St. Augustinus.

We identified all cases of CRC liver metastases (CRCLMs) resected from patients treated preoperatively with a combination of bevacizumab and chemotherapy (bev-chemo) at RM from 2006-2012 (101 metastases from 47 patients). Of these, 59 liver metastases from 33

patients were eligible for our study correlating HGP with pathological response. A consort diagram illustrates how these 59 cases were selected for inclusion (Supplementary Fig. 2). For patient characteristics see Supplementary Table 1. For correlating HGP with morphological response on imaging, 52 lesions from 31 patients were eligible for inclusion (Supplementary Fig. 2). For correlating HGP with response by RECIST criteria all 59 liver metastases from 33 patients were eligible for inclusion.

We identified all CRCLMs resected from patients treated preoperatively with bev-chemo at MUHC from 2008–2014 (191 CRC liver metastases from 65 patients). Of these, 128 liver metastases from 59 patients were eligible for correlating HGP with pathological response (Supplementary Fig. 4). For patient characteristics see Supplementary Table 3. For the analysis of new CRCLMs (i.e. lesions that only presented after the initiation of bev-chemo but were not present on baseline scans) we identified 35 resected lesions from 13 patients treated preoperatively with bev-chemo at MUHC (Supplementary Fig. 4). For patient characteristics see Supplementary Table 6. A total of 148 liver metastases from 62 patients treated preoperatively with bev-chemo were eligible for correlating HGP with overall survival. For the analysis of CRC liver metastases from patients that did not receive pre-operative therapy, we identified 32 lesions from 19 patients at MUHC. For patient characteristics see Supplementary Table 7. For the analysis of CRCLMs from patients treated with chemotherapy alone we identified all cases of CRCLMs resected from patients treated preoperatively with chemotherapy at MUHC from 2008–2014 (81 metastases resected from 30 patients) and from this group a total of 76 liver metastases from 29 patients were eligible for our study correlating HGP with overall survival.

For breast cancer, all breast cancer liver metastasis cases obtained via resection or autopsy at GZA Hospitals St. Augustinus from 2004–2015 were examined (17 patients). For patient characteristics see Supplementary Table 11.

Therapy administration

Patients receiving treatment with bevacizumab in combination with chemotherapy were treated with one the following regimens.

CAPOX plus bevacizumab: 21 day treatment cycle consisting of 15 minute intravenous infusion of bevacizumab (7.5 mg per kg) and 2 hour intravenous infusion of oxaliplatin (130 mg per m^2) on day one, followed by daily oral capecitabine (1700 mg per m^2) in two divided doses from days 1 to 14.

FOLFOX plus bevacizumab: 14 day treatment cycle consisting of 10 minute intravenous infusion of bevacizumab (5 mg per kg), 2 hour intravenous infusion of oxaliplatin (85 mg per m^2), 2 hour intravenous infusion of folinic acid (400 mg per m^2) with a bolus dose of 5-FU (400 mg per m^2) on day one, followed by 48 hour continuous intravenous infusion of 5-FU (1200 mg per m^2 per day).

FOLFIRI plus bevacizumab: 14 day treatment cycle consisting of 10 minute intravenous infusion of bevacizumab (5 mg per kg), 1 hour intravenous infusion of irinotecan (180 mg per m^2), 1 hour intravenous infusion of folinic acid (400 mg per m^2) with a bolus dose of 5-

FU (400 mg per m^2) on day one, followed by 48 hour continuous intravenous infusion of 5-FU (1200 mg per m^2 per day).

For patients that received chemotherapy alone, most patients received either FOLFOX or FOLFIRI administered as described above without the addition of bevacizumab. However, a minority of patients that received chemotherapy alone received one of the following regimens instead.

FOLFIRINOX: 14 day treatment cycle consisting of oxaliplatin (85 mg per m^2), irinotecan (180 mg per m^2), leucovorin (400 mg per m^2), and 5-FU (400 mg per m^2) followed by a 48 hour continuous intravenous infusion of 5-FU (1200 mg per m^2 per day).

5-FU: 14 day treatment cycle consisting of leucovorin (400 mg per m^2) and 5-FU (400 mg per m^2) followed by 48 hour continuous intravenous infusion of 5-FU (1200 mg per m^2 per day).

The decision to administer therapy, the type of therapy and the number of cycles were based on the recommendation of the local multidisciplinary team. Patients received oxaliplatin- or irinotecan-based regimens with the addition of bevacizumab preferentially, as long as there were no contraindications to administer bevacizumab, such as uncontrolled hypertension, history of gastrointestinal perforation, history of arterial or venous thromboembolic events, history of significant bleeding, recent surgery or nephrotic syndrome. In the case that the patient was deemed unsuitable for administration of bevacizumab, the patient received chemotherapy alone.

Scoring HGPs

Sections (5 μm thickness) were prepared from formalin fixed paraffin-embedded (FFPE) liver resection specimens, stained with H&E and then scored for HGP by two pathologists with extensive experience of scoring the HGPs. In brief, the tumor-liver interface was categorized as being desmoplastic, pushing or replacement HGP according to the following criteria. Desmoplastic HGP: there was no direct contact between cancer cells and liver parenchyma and the cancer cells were separated from the liver parenchyma by a layer of desmoplastic stroma. Pushing HGP: close contact between cancer cells and normal liver tissue was observed, without an intervening desmoplastic stroma. The normal liver was compressed by the tumor and no invasion of cancer cells into the hepatic plates was observed. Replacement HGP: close contact between cancer cells and liver parenchyma was observed, without an intervening desmoplastic stroma. The cancer cells invaded into the hepatic plates and replaced the hepatocytes without destroying the vascular architecture of the liver at the tumor-liver interface.

Given that some lesions present with a mixture of different HGPs, the percentage of the tumor-liver interface with a desmoplastic, pushing or replacement HGP was scored in intervals of 5% in all available tissue blocks. Where multiple blocks were available, the mean average score was calculated to produce a single score for % desmoplastic, % pushing and % replacement for each lesion.

In some cases, invasion of cancer cells into the hepatic plates (which is a defining feature of the replacement HGP and required for vessel co-option) was also accompanied by compression of the liver parenchyma. These cases were scored as replacement HGP and not pushing HGP. This subtle but important refinement to the criteria for scoring the HGPs helps to explain why, in the current study, the incidence of the replacement HGP in CRC metastases is higher than in some previous studies.

Agreement of HGP scores

The level of intra-observer and inter-observer agreement for scoring the HGPs was tested independently. In brief, two pathologists (observers A and B) scored the HGP (% replacement, % desmoplastic and % pushing) in 150 tissue sections of resected CRCLM without conferring. After a break of several weeks, the two pathologists scored the same set of 150 tissue sections again without conferring and without reference to their previous scores. The % replacement scores from each round of scoring were then used to test the level of intra- and inter-observer agreement. The difference between scores is plotted in Supplementary Fig. 16.

The correlation between scores was calculated using Pearson's correlation co-efficient. We also analyzed the data using Bland-Altman plots (Supplementary Fig. 17) from which we determined the mean difference between the scores and the limits of agreement (2 standard deviations from the mean difference)[52]. The results are tabulated in Supplementary Table 12.

There was a strong correlation ($r > 0.98$) between the scores recorded by the same observer (intra-observer agreement), and also a strong correlation ($r > 0.96$) between the scores recorded by the two different observers (inter-observer agreement). The Bland-Altman plots showed that the mean difference between the scores recorded by the same observer was small (0.033 and −0.633 and that the mean difference between the scores recorded by the two different observers was also small (−1.500 and −2.167). Taken together, these data indicate that there is a good level of inter- and intra-observer agreement between observers for scoring the HGPs.

Despite this fact, the limits of agreement for the inter-observer agreement are quite wide (−22.88 to 19.88 and −25.287 to 20.953). This occurred due to the presence of some cases which have a 'mixed' growth pattern that can be more difficult to score and led to some divergent scores. However, in the main study, in any cases having a 'mixed' growth pattern where there was a significant disagreement between observers, the two observers were always able to reconcile their differences in order to produce a single consensus score for the lesion.

Scoring of pathological response to therapy

For scoring of the pathological response to bev-chemo from H&E-stained specimens, the extent of viable carcinoma was assessed semi-quantitatively as a percentage relative to the total tumor surface area. Each lesion was assigned as belonging to one of four categories: >75%, 50–75%, 25–49% or <25% viable carcinoma[53], with areas of 'usual necrosis' being considered part of the viable tumor fraction, whilst areas of 'infarct-like necrosis' were

considered to be non-viable[54]. Pathological response was scored independently by three experienced pathologists using these criteria. Any difference in score that occurred between pathologists was resolved by consensus to produce a single score for each lesion.

Scoring of morphological response to therapy

Pre- and post-treatment contrast-enhanced CT scans of suitable quality were available for 52 lesions from 31 patients for this analysis (see consort diagram, Supplementary Fig. 2) and the response to therapy was evaluated using a method based on previously published morphological response criteria[18,20] as described below.

The appearance of each lesion on both the pre- and post-treatment scan was scored as belonging to one of three morphology groups (group-1, group-2 or group-3). A homogeneous, low attenuation lesion with a thin, sharply defined tumor-liver interface was defined as group-1. A lesion having heterogeneous attenuation and a thick, poorly defined tumor-liver interface was defined as group-3. A lesion that was intermediate between group-1 and group-3, having a moderate degree of heterogeneous attenuation and a moderately defined tumor-liver interface, was defined as group-2.

Morphological response was defined as an optimal response (OR) if the lesion changed from a group-3 or group-2 to a group-1 following treatment; a partial response (PR) if the lesion changed from group-3 to group-2 following treatment; and an absent response (AR) if the metastasis either did not change group, or went from group-2 to group-3, following treatment. Morphological response was scored independently by two observers. Any difference in scores was resolved by consensus to produce a single score for each lesion. Lesions scored as AR were considered to be poor responders, whilst lesions scored as PR or OR were considered to be good responders. Scorers were blinded as to the HGP and pathological response data.

Scoring of response by RECIST

Change in lesion size was determined from MRI scan data, by calculating the change in lesion diameter that occurred between the pre- and post-treatment scans. The lesion size measurements were obtained from the patient records and were therefore blinded, because the original reporting radiologist had no prior knowledge of our retrospective HGP and pathological response data. For this analysis, MRI scans of suitable quality were available for 59 lesions from 33 patients. Lesions were classified as partial response (PR), stable disease (SD) or progressive disease (PD) according to the following criteria: PR (lesion underwent 30% decrease in size between pre- and post-treatment scan), SD (lesion underwent <30% decrease in size and <20% increase in size between pre- and post-treatment scan) and PD (lesion underwent 20% increase in size between pre- and post-treatment scan).

Kaplan-Meier estimates of overall survival

Patients were allocated to one of three groups: predominant replacement, predominant desmoplastic or predominant pushing. To allocate patients to each group, the mean percentage of replacement, desmoplastic and pushing HGP was calculated for each patient

using the data available from all lesions. Patients with a mean replacement HGP of >50% were allocated to the predominant replacement group, patients with a mean desmoplastic HGP of >50% were allocated to the predominant desmoplastic group and patients with a mean pushing HGP of >50% were allocated to the predominant pushing group. This method allowed unambiguous allocation of patients to the three groups (i.e. there were no patients scored as having a 50:50 score for two growth patterns). Overall survival estimates were calculated from the date of diagnosis of liver metastases to the date of death or to the date of last follow-up.

Immunohistochemistry

Sections of 5 μm thickness were prepared from FFPE blocks, de-paraffinized and rehydrated by standard protocols. Depending on the antibodies used, antigen retrieval was performed either at pH 6 in a pressure cooker (Menapath Access Retrieval Unit, Menarini Diagnostics) or at pH 9 in a microwave. Sections were incubated in blocking buffer (1% BSA in PBS-T) for 1 hour followed by incubation with primary antibodies in blocking buffer for 2 hours, all at room temperature. Primary antibodies used were: mouse anti-ARPC3 (Millipore, MABT95; dilution 1:2500), mouse anti-human CD31 (Dako, M0823; dilution 1:30), rabbit anti-mouse CD31 (Dianova, DIA310; dilution 1:75), rabbit anti-collagen-3 (Abcam, ab7778; dilution 1:200), mouse anti-cytokeratin-19 (Dako, M0888; dilution 1:100), mouse anti-cytokeratin-20 (Dako, M7019; dilution 1:50), mouse anti-estrogen receptor alpha (ER) (Dako, M3643, dilution 1:80), mouse anti-hepatocyte specific antigen (Santa Cruz Biotechnology, sc-58693; dilution 1:400), mouse anti-pan-cytokeratin (Dako, M3515, dilution 1:75), rabbit anti-pan-cytokeratin (Dako, Z0622; dilution 1:400), mouse anti-Ki67 (Dako, M7240; dilution 1:300), mouse anti-progesterone receptor (PgR) (Dako, M3643; dilution 1:200) and rabbit anti-αSMA (Abcam, ab5694; dilution 1:500). Antibody validation is provided on the manufacturers' websites. For immunofluorescence, primary antibodies were detected with Alexa-488 or Alexa-555 fluorescently-conjugated secondary antibodies (Invitrogen) diluted in blocking buffer supplemented with DAPI for 30 mins at room temperature, followed by mounting under glass coverslips in MOWIOL mountant supplemented with anti-fade (0.1% w/v 1,4-diazabicyclo[2.2.2]octane) (Sigma). For DAB and TMB staining, primary antibodies were detected with Envision Flex system (K8002, Dako), followed by a light counterstain with hematoxylin before mounting under glass coverslips in DPEX mountant. For HER2 we used the HercepTest kit (SK001, Dako). Images were captured using a confocal laser-scanning microscope (Leica) or a light microscope (Olympus), as appropriate.

Scoring subtypes of breast cancer

Cases of breast cancer liver metastasis were characterized for intrinsic molecular subtype as per published guidelines55. In brief, FFPE sections were stained for ER, PgR, HER2 or Ki67 and scored by a pathologist. For both ER and PgR, positive staining in 1% of tumor cell nuclei was required in order for the case to be considered receptor positive56. For HER2, the following system was utilized: 0 or 1[+] (HER2 negative), 2[+] (HER2 borderline), or 3[+] (HER2 positive)57. HER2 borderline cases underwent additional testing using HER2 CISH pharmDx kit (SK109, Dako) to test for HER2 amplification. The presence of HER2 amplification was considered to indicate that the case was HER2 positive. Cases were

deemed Ki67 'low' if <14% of nuclei were Ki67 positive, otherwise they were considered to be Ki67 'high.' The results of the ER, PgR, HER2 and Ki67 analysis were then used to assign each case to an intrinsic molecular subtype according to the criteria recommended by Goldhirsch *et al* 55 as detailed in Supplementary Table 13.

Cell culture

Luciferase-tagged HT29 cells (HT-29-luc2 from Caliper Life Sciences) were authenticated by STR typing and regularly tested for mycoplasma and shown to be contamination free. They were cultured in DMEM supplemented with 10% FCS, L-glutamine and penicillin/ streptomycin at 37°C in an atmosphere of 5% CO_2.

shRNA knockdown

HT29 cells were stably transduced with shRNA oligonucleotides using lentiviral particles. We utilized three different shRNA oligonucleotides designed to target ARPC3 (shARPC3-1, shARPC3-1, shARPC3-1) and a control oligonucleotide with a validated non-targeting sequence (control shRNA) as follows:

shARPC3-1 (5'CACCCGCTTAATAAGAATAAGTACGAATACTTATTCTTATTAAGCG3')

shARPC3-2 (5'CACCGAAATGTATACGCTGGGAATCCGAAGATTCCCAGCGTATACATTTC3')

shARPC3-3 (5'CACCGCCAAGGTGAGAAAGAAATGTCGAAACATTTCTTTCTCACCTTGGC3')

control shRNA (5'CACCTAAGGCTATGAAGAGATACCG AAGTATCTCTTCATAGCCTTA3')

Oligonucleotides were ligated into the pENTR/U6 Gateway system entry vector (Invitrogen) according to the manufacturer's instructions. Oligonucleotide sequences were verified by sequencing and then transferred, together with the U6 promoter, into the Gateway-modified pSEW lentiviral vector (this vector also contains the EGFP gene under the control of an independent SFFV promoter). Viral supernatants were generated by lipofectamine-2000 co-transfection of this expression vector and two packaging vectors (psPAX2 and pMD2.G) into HEK293T cells. Viral supernatants were collected and stored at -80°C until use. Adherent HT29 cells were infected with viral supernatant for 24 hours. Following this, the infecting medium was aspirated and replaced by DMEM complete. At 3–5 days after infection, HT29 cells were trypsinized and sorted for GFP expression by flow cytometry on a FACS ARIA instrument (BD Biosciences).

Western blotting

Western blotting was performed as described58. In brief, cell lysates were separated on 10% SDS-PAGE gels at 150 V for 1 hour. Transfer to nitrocellulose membranes was performed at 100 V for 1 hour. Membranes were blocked using blocking buffer (TBS-T supplemented with 5% milk) and then probed with anti-ARPC3 antibodies (Santa Cruz Biotechnology, sc-136020; dilution 1:200) or anti-HSC70 antibodies (Santa Cruz Biotechnology, sc-7298;

dilution 1:20,000). After incubation with HRP-conjugated secondary antibodies in blocking buffer, membranes were incubated with chemiluminescence substrate and exposed to films. Densitometry was performed using ImageJ software on three independent western blots. Expression levels of ARPC3 were normalized to the expression level of HSC-70. Antibody validation is provided on the manufacturer's website.

Cell motility assay

Cells were plated at a density of 50,000 cells per well in a 6-well plate. After 24 hours, the media was refreshed and the plates were transferred to the stage of an inverted Leica IX-70 time-lapse microscope at 37°C in an atmosphere containing 5% CO_2. Images were captured through a 20X phase contrast objective every 30 minutes for 48 hours. To measure cell migration, random cells were tracked in time-lapse videos for 30 hours using the manual tracking plugin in ImageJ. For the purposes of quantification, 30 cells from each experimental group were analyzed from across two independent experiments. Results were expressed in terms of cell velocity (μm per minute).

Cell proliferation assay

To assess the proliferation kinetics of cells, 2000 HT29 cells were seeded (in quadruplicate wells) on to four different 96-well plates (plates 1 to 4). Cell viability was measured from plates 1, 2, 3 and 4 at 24, 48, 72 and 96 hours, respectively, using the CellTitre-Glo reagent (Promega) according to the manufacturer's instructions. The quantity of viable cells was expressed relative to the signal at 24 hours from three independent experiments.

Preclinical model of advanced liver metastasis

The Institute of Cancer Research Animal Ethics Committee granted approval for animal work. Procedures were performed in accordance with United Kingdom Home Office regulations. We used female CB17 SCID mice (CB17/lcr-*Prkdc^scid*/lcrlcoCrl) at 12–16 weeks of age (obtained from Charles River UK). Parental HT29 cells, or HT29 cells stably transduced with shRNA constructs, were resuspended in growth factor-reduced Matrigel (Invitrogen) at a concentration of $1x10^7$ cells per ml. Cells were introduced into the liver by laparotomy performed under general anesthesia (inhaled isoflurane). A midline incision was made through the peritoneum and the left main lobe of the liver was exteriorized. This lobe was injected with $4x10^5$ cells in a volume of 40 μL using a 29-gauge needle and then returned to the peritoneal cavity, followed by closure of the wound. In order to assess the effect of ARPC3 knockdown on the HGP (Fig. 6e) mice were culled 21 days post-injection of cancer cells. The tumor-bearing liver lobe was harvested, fixed in formalin and embedded in paraffin.

For experiments where treatment was administered (Fig. 6f–h and Supplementary Fig. 15), we waited for 10 days post- injection to allow for tumor establishment. At 10 days, mice were injected subcutaneously with 75 mg per kg D-luciferin (Caliper Life Sciences), anesthetized with isoflurane and then imaged in an Lumina II™ IVIS (*In Vivo* Imaging System) instrument (Caliper Life Sciences). Quantification of liver bioluminescence was performed using Living Image™ software (Caliper Life Sciences) according to

manufacturer's instructions. The bioluminescence measurement was used to ensure that subjects of equivalent tumor burden were allocated to each experimental group.

Capecitabine powder (LC Laboratories) was dissolved in vehicle for oral administration (40 mM citrate buffer pH 6, 5% gum Arabic). B20-4.1.1 (Genentech), an antibody that blocks both mouse and human VEGF-A28, was formulated in sterile PBS for intraperitoneal administration. One cycle of therapy consisted of the following: mice received 500 mg per kg capecitabine or vehicle by oral gavage every day for 5 days, followed 2 days treatment break, with intraperitoneal injection of 2.5 mg per kg B20-4.1.1 or vehicle on the first and fifth day of the cycle. In mice that received capecitabine alone, the same protocol was followed but without the administration of B20-4.1.1. Mice were administered two cycles of therapy and then culled at 24 days post-injection of cancer cells. The tumor-bearing liver lobe was harvested, fixed in formalin and embedded in paraffin.

For quantification of tumor burden, H&E-stained sections were prepared. Sections were digitally scanned (Nanozoomer, Hamamatsu) and imported into NDPI viewer software (Hamamatsu). The marquee tool was used freehand to create regions of interest (ROIs) around areas of tumor in the section and tumor burden measurement was calculated in terms of area in mm^2. For quantification of vessel density, sections were co-stained for CD31 (detected with TMB) and CK20 (detected with DAB). Tumor vessels were manually counted and expressed in terms of vessels per mm^2 of tumor area. H&E-stained sections were scored for HGP according to the same criteria used for human samples of liver metastasis. The scoring of tumor burden, vessel density and HGPs was performed in a blinded fashion. The number of mice per group was selected based on prior experience regarding the minimum number of animals necessary to detect a statistically significant difference between experimental groups. No randomization method was used.

ARPC3 staining

HT29 cells stably transfected with the control shRNA or shARPC3-3 were grown to confluency, washed in PBS, harvested by trypsinization and then pelleted by centrifugation. Pelleted cells (approximately $1x10^7$ cells per pellet) were then resuspended in formalin and fixed for 15 minutes followed by pelleting again and embedding in paraffin. Tissue sections were prepared and then stained using anti-ARPC3 antibody (Millipore, MABT95; dilution 1:2500) as described above (see Immunohistochemistry) with antigen retrieval performed in pH 6 citrate buffer with heating in a microwave for 18 minutes.

The same staining protocol was used to stain for ARPC3 in FFPE tissue sections of human liver metastasis specimens. Positive staining for ARPC3 was observed in cancer cells and in some stromal cell types (including immune cells and Kuppfer cells), but only cancer cell staining was scored. The scoring of ARPC3 staining intensity in cancer cells was performed semi-quantitatively by a pathologist. For each case examined, the percentage of cancer cells having 1^+ (weak), 2^+ (moderate) or 3^+ (strong) staining intensity was scored. The result for each case was expressed as an H-score as calculated by the formula: (% area of weak staining) + (2 x % area of moderate staining) + (3 x % area of strong staining). This generated a score between 0 - 300 for each case.

Statistical analysis

The univariate analysis of clinical data reported in Figs. 1 and 2, in Supplementary Figs. 3, 5, 6, 7 and 8, and in Supplementary Tables 2, 4, 9 and 10 was performed using the two-tailed χ^2 test. A univariate and multivariate analysis on 181 lesions from 90 patients was performed to determine clinical characteristics significantly associated with a good pathological response. Given that some lesions came from the same patient, a generalized estimating equation (GEE) approach was used to account for the within-patient covariance (exchangeable working correlation structure was used to specify the correlation among lesions clustered within the same patient). A total of 12 different clinical variables were included in the univariate analysis. Only 5 variables which met a pre-defined threshold for association with pathological response in the univariate GEE analysis (*P*-value <0.25) were then included in the subsequent multivariate GEE analysis. The results of the analysis are reported in Supplementary Table 5.

For the overall survival data, the Log-Rank test was used to determine the statistical signficance and Cox proportional hazards regression was used to determine hazard ratios (Fig. 4b–e). A univariate and multivariate analysis to determine clinical characteristics associated with overall survival was performed using the Cox proportional hazards regression model. A total of 12 different clinical variables were included in the univariate analysis. Only 2 variables which met a pre-defined threshold for association with overall survival in the univariate analysis (*P*-value <0.25) were then included in the subsequent multivariate analysis. The results of the analysis are reported in Supplementary Table 8. The proportional hazards assumption for the Cox regression models was tested based on weighted Schoenfeld residuals[59]: for the overall survival analyses (Fig. 4b–e) the *P*-values calculated ranged from 0.09 to 0.69, for the univariate analyses the *P*-values calculated ranged from 0.08 to 0.99 (depending on the variable), whilst the global *P*-value calculated for the multivariate analysis was 0.85, indicating that the proportional hazards ratio assumption was not rejected in any instance.

Where appropriate, the Kolmogorov-Smirnov normality test was used to determine the normality of the data and the F-test equality of variances test was used to determine whether the variance between groups was similar. For normally distributed data, we used two-tailed unpaired Student's t-test (with Welch's correction applied if the variance between groups was not similar) to compare experimental groups (Fig. 6g,h and Supplementary Figs. 11h and 15b,c). For non-normally distributed data we used Kruskal-Wallis test (Fig. 4a) or Mann-Whitney U-test (Fig. 6d-f and Supplementary Fig. 15a) to compare experimental groups. For data where the sample number was too small (n = 3 independent experiments) to determine normality, but where the variance between groups was similar, we used two-tailed unpaired Student's t-test to compare experimental groups (Fig. 6c and Supplementary Fig. 13). Intra- and inter-observer agreement for scoring the HGPs was analyzed using Pearson's correlation co-efficient and Bland-Altman plots (Supplementary Fig. 17). For all statistical analyses, *P*-values below 0.05 were considered statistically significant.

Supplementary Material

Refer to Web version on PubMed Central for supplementary material.

Acknowledgments

References

1. Ferrara N, Hillan KJ, Gerber HP, Novotny W. Discovery and development of bevacizumab, an anti-VEGF antibody for treating cancer. Nat Rev Drug Discov. 2004; 3:391–400. [PubMed: 15136787]

2. Kerbel RS. Tumor angiogenesis. N Engl J Med. 2008; 358:2039–2049. [PubMed: 18463380]

3. Hurwitz H, et al. Bevacizumab plus irinotecan, fluorouracil, and leucovorin for metastatic colorectal cancer. The New England journal of medicine. 2004; 350:2335–2342. [PubMed: 15175435]

4. Cunningham D, et al. Bevacizumab plus capecitabine versus capecitabine alone in elderly patients with previously untreated metastatic colorectal cancer (AVEX): an open-label, randomised phase 3 trial. Lancet Oncol. 2013; 14:1077–1085. [PubMed: 24028813]

5. Ebos JM, Kerbel RS. Antiangiogenic therapy: impact on invasion, disease progression, and metastasis. Nat Rev Clin Oncol. 2011; 8:210–221. [PubMed: 21364524]

6. Vasudev NS, Reynolds AR. Anti-angiogenic therapy for cancer: current progress, unresolved questions and future directions. Angiogenesis. 2014; 17:471–494. [PubMed: 24482243]

7. Pezzella F, et al. Angiogenesis in primary lung cancer and lung secondaries. Eur J Cancer. 1996; 32A:2494–2500. [PubMed: 9059338]

8. Vermeulen PB, et al. Liver metastases from colorectal adenocarcinomas grow in three patterns with different angiogenesis and desmoplasia. The Journal of pathology. 2001; 195:336–342. [PubMed: 11673831]

9. Dome B, Hendrix MJ, Paku S, Tovari J, Timar J. Alternative vascularization mechanisms in cancer: Pathology and therapeutic implications. Am J Pathol. 2007; 170:1–15. [PubMed: 17200177]

10. Donnem T, et al. Vessel co-option in primary human tumors and metastases: an obstacle to effective anti-angiogenic treatment? Cancer Med. 2013; 2:427–436. [PubMed: 24156015]

11. Jayson GC, Kerbel R, Ellis LM, Harris AL. Antiangiogenic therapy in oncology: current status and future directions. Lancet. 2016

12. Adams RB, et al. Selection for hepatic resection of colorectal liver metastases: expert consensus statement. HPB (Oxford). 2013; 15:91–103. [PubMed: 23297719]

13. Van den Eynden GG, et al. The multifaceted role of the microenvironment in liver metastasis: biology and clinical implications. Cancer research. 2013; 73:2031–2043. [PubMed: 23536564]

14. Stessels F, et al. Breast adenocarcinoma liver metastases, in contrast to colorectal cancer liver metastases, display a non-angiogenic growth pattern that preserves the stroma and lacks hypoxia. Br J Cancer. 2004; 90:1429–1436. [PubMed: 15054467]

15. Gruenberger B, et al. Bevacizumab, capecitabine, and oxaliplatin as neoadjuvant therapy for patients with potentially curable metastatic colorectal cancer. J Clin Oncol. 2008; 26:1830–1835. [PubMed: 18398148]

16. Chaudhury P, et al. Perioperative chemotherapy with bevacizumab and liver resection for colorectal cancer liver metastasis. HPB. 2010; 12:37–42. [PubMed: 20495643]

17. Wong R, et al. A multicentre study of capecitabine, oxaliplatin plus bevacizumab as perioperative treatment of patients with poor-risk colorectal liver-only metastases not selected for upfront resection. Ann Oncol. 2011; 22:2042–2048. [PubMed: 21285134]

18. Chun YS, et al. Association of computed tomography morphologic criteria with pathologic response and survival in patients treated with bevacizumab for colorectal liver metastases. JAMA. 2009; 302:2338–2344. [PubMed: 19952320]

19. Shindoh J, et al. Optimal morphologic response to preoperative chemotherapy: an alternate outcome end point before resection of hepatic colorectal metastases. J Clin Oncol. 2012; 30:4566–4572. [PubMed: 23150701]

20. Boonsirikamchai P, et al. CT findings of response and recurrence, independent of change in tumor size, in colorectal liver metastasis treated with bevacizumab. AJR American journal of roentgenology. 2011; 197:W1060–1066. [PubMed: 22109320]

21. Van den Eynden GG, et al. The histological growth pattern of colorectal cancer liver metastases has prognostic value. Clin Exp Metastasis. 2012; 29:541–549. [PubMed: 22476470]

22. Nurnberg A, Kitzing T, Grosse R. Nucleating actin for invasion. Nature reviews. 2011; 11:177–187.

23. Otsubo T, et al. Involvement of Arp2/3 complex in the process of colorectal carcinogenesis. Modern pathology : an official journal of the United States and Canadian Academy of Pathology Inc. 2004; 17:461–467.

24. Iwaya K, et al. Correlation between liver metastasis of the colocalization of actin-related protein 2 and 3 complex and WAVE2 in colorectal carcinoma. Cancer science. 2007; 98:992–999. [PubMed: 17459058]

25. Kopetz S, et al. Synergistic activity of the SRC family kinase inhibitor dasatinib and oxaliplatin in colon carcinoma cells is mediated by oxidative stress. Cancer research. 2009; 69:3842–3849. [PubMed: 19383922]

26. Nyati MK, et al. The potential of 5-fluorocytosine/cytosine deaminase enzyme prodrug gene therapy in an intrahepatic colon cancer model. Gene therapy. 2002; 9:844–849. [PubMed: 12080378]

27. Gray MJ, et al. Therapeutic targeting of Id2 reduces growth of human colorectal carcinoma in the murine liver. Oncogene. 2008; 27:7192–7200. [PubMed: 18806828]

28. Liang WC, et al. Cross-species vascular endothelial growth factor (VEGF)-blocking antibodies completely inhibit the growth of human tumor xenografts and measure the contribution of stromal VEGF. J Biol Chem. 2006; 281:951–961. [PubMed: 16278208]

29. Miller KD, et al. Randomized phase III trial of capecitabine compared with bevacizumab plus capecitabine in patients with previously treated metastatic breast cancer. J Clin Oncol. 2005; 23:792–799. [PubMed: 15681523]

30. Miller K, et al. Paclitaxel plus bevacizumab versus paclitaxel alone for metastatic breast cancer. The New England journal of medicine. 2007; 357:2666–2676. [PubMed: 18160686]

31. Miles DW, et al. Phase III study of bevacizumab plus docetaxel compared with placebo plus docetaxel for the first-line treatment of human epidermal growth factor receptor 2-negative metastatic breast cancer. J Clin Oncol. 2010; 28:3239–3247. [PubMed: 20498403]

32. Robert NJ, et al. RIBBON-1: randomized, double-blind, placebo-controlled, phase III trial of chemotherapy with or without bevacizumab for first-line treatment of human epidermal growth factor receptor 2-negative, locally recurrent or metastatic breast cancer. J Clin Oncol. 2011; 29:1252–1260. [PubMed: 21383283]

33. Brufsky AM, et al. RIBBON-2: a randomized, double-blind, placebo-controlled, phase III trial evaluating the efficacy and safety of bevacizumab in combination with chemotherapy for second-line treatment of human epidermal growth factor receptor 2-negative metastatic breast cancer. J Clin Oncol. 2011; 29:4286–4293. [PubMed: 21990397]

34. Naresh KN, Nerurkar AY, Borges AM. Angiogenesis is redundant for tumour growth in lymph node metastases. Histopathology. 2001; 38:466–470. [PubMed: 11422485]

35. Jeong HS, et al. Investigation of the Lack of Angiogenesis in the Formation of Lymph Node Metastases. J Natl Cancer Inst. 2015; 107

36. Colpaert CG, et al. Cutaneous breast cancer deposits show distinct growth patterns with different degrees of angiogenesis, hypoxia and fibrin deposition. Histopathology. 2003; 42:530–540. [PubMed: 12786888]

37. Breast-Cancer-Progression-Working-Party. Evidence for novel non-angiogenic pathway in breast-cancer metastasis. Lancet. 2000; 355:1787–1788. [PubMed: 10832831]

38. Szabo V, et al. Mechanism of tumour vascularization in experimental lung metastases. The Journal of pathology. 2015; 235:384–396. [PubMed: 25319725]

39. Carbonell WS, Ansorge O, Sibson N, Muschel R. The vascular basement membrane as "soil" in brain metastasis. PLoS One. 2009; 4:e5857. [PubMed: 19516901]

40. Bugyik E, et al. Lack of angiogenesis in experimental brain metastases. J Neuropathol Exp Neurol. 2011; 70:979–991. [PubMed: 22002424]

41. Valiente M, et al. Serpins promote cancer cell survival and vascular co-option in brain metastasis. Cell. 2014; 156:1002–1016. [PubMed: 24581498]

42. Jain RK, et al. Biomarkers of response and resistance to antiangiogenic therapy. Nat Rev Clin Oncol. 2009; 6:327–338. [PubMed: 19483739]

43. Kuczynski EA, et al. Co-option of Liver Vessels and Not Sprouting Angiogenesis Drives Acquired Sorafenib Resistance in Hepatocellular Carcinoma. J Natl Cancer Inst. 2016; 108

44. Rubenstein JL, et al. Anti-VEGF antibody treatment of glioblastoma prolongs survival but results in increased vascular cooption. Neoplasia. 2000; 2:306–314. [PubMed: 11005565]

45. Kusters B, et al. Vascular endothelial growth factor-A(165) induces progression of melanoma brain metastases without induction of sprouting angiogenesis. Cancer research. 2002; 62:341–345. [PubMed: 11809675]

46. Leenders WP, et al. Antiangiogenic therapy of cerebral melanoma metastases results in sustained tumor progression via vessel co-option. Clin Cancer Res. 2004; 10:6222–6230. [PubMed: 15448011]

47. Paez-Ribes M, et al. Antiangiogenic therapy elicits malignant progression of tumors to increased local invasion and distant metastasis. Cancer Cell. 2009; 15:220–231. [PubMed: 19249680]

48. de Groot JF, et al. Tumor invasion after treatment of glioblastoma with bevacizumab: radiographic and pathologic correlation in humans and mice. Neuro Oncol. 2010; 12:233–242. [PubMed: 20167811]

49. Lu KV, et al. VEGF Inhibits Tumor Cell Invasion and Mesenchymal Transition through a MET/VEGFR2 Complex. Cancer Cell. 2012; 22:21–35. [PubMed: 22789536]

50. Sennino B, et al. Suppression of Tumor Invasion and Metastasis by Concurrent Inhibition of c-Met and VEGF Signaling in Pancreatic Neuroendocrine Tumors. Cancer Discov. 2012; 2:270–287. [PubMed: 22585997]

51. Depner C, et al. EphrinB2 repression through ZEB2 mediates tumour invasion and anti-angiogenic resistance. Nature communications. 2016; 7:12329.

52. Bland JM, Altman DG. Statistical methods for assessing agreement between two methods of clinical measurement. Lancet. 1986; 1:307–310. [PubMed: 2868172]

53. Ribero D, et al. Bevacizumab improves pathologic response and protects against hepatic injury in patients treated with oxaliplatin-based chemotherapy for colorectal liver metastases. Cancer. 2007; 110:2761–2767. [PubMed: 17960603]

54. Chang HH, Leeper WR, Chan G, Quan D, Driman DK. Infarct-like necrosis: a distinct form of necrosis seen in colorectal carcinoma liver metastases treated with perioperative chemotherapy. The American journal of surgical pathology. 2012; 36:570–576. [PubMed: 22301494]

55. Goldhirsch A, et al. Personalizing the treatment of women with early breast cancer: highlights of the St Gallen International Expert Consensus on the Primary Therapy of Early Breast Cancer 2013. Ann Oncol. 2013; 24:2206–2223. [PubMed: 23917950]

56. Hammond ME, et al. American Society of Clinical Oncology/College of American Pathologists guideline recommendations for immunohistochemical testing of estrogen and progesterone receptors in breast cancer (unabridged version). Archives of pathology & laboratory medicine. 2010; 134:e48–72. [PubMed: 20586616]

57. Wolff AC, et al. Recommendations for human epidermal growth factor receptor 2 testing in breast cancer: American Society of Clinical Oncology/College of American Pathologists clinical practice guideline update. J Clin Oncol. 2013; 31:3997–4013. [PubMed: 24101045]

58. Gourlaouen M, Welti JC, Vasudev NS, Reynolds AR. Essential role for endocytosis in the growth factor-stimulated activation of ERK1/2 in endothelial cells. J Biol Chem. 2013; 288:7467–7480. [PubMed: 23341459]

59. Grambsch PM, Therneau TM. Proportional Hazards Tests and Diagnostics Based on Weighted Residuals. Biometrika. 1994; 81:515–526.
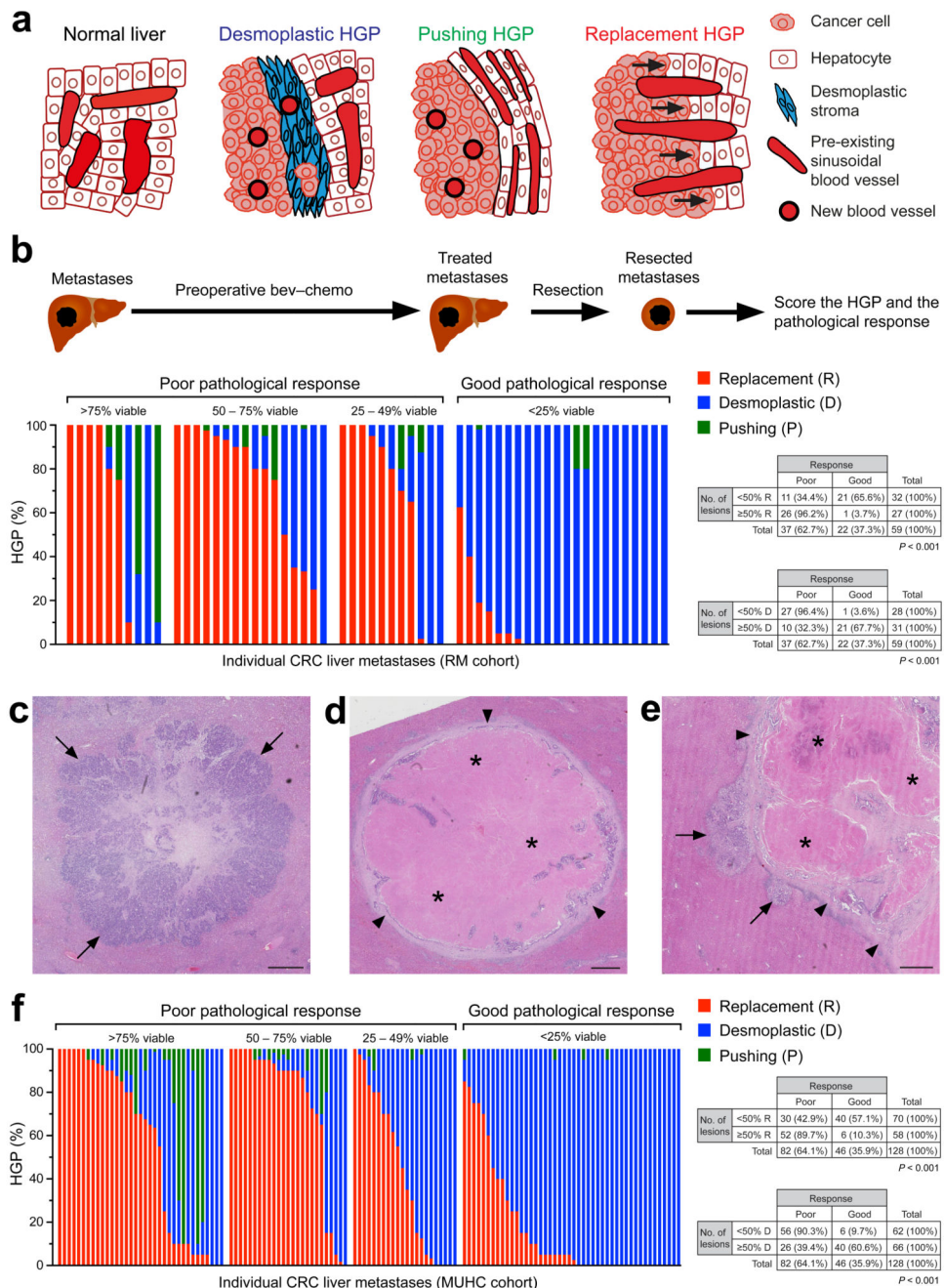
Figure 1. Correlation between HGP and pathological response in patients treated preoperatively with bevacizumab

a. Diagrams illustrating the morphology of the normal liver or the morphology of the tumor-liver interface in liver metastases with a desmoplastic, pushing or replacement HGP. **b.** The HGPs and the pathological response to bev-chemo were scored in 59 CRCLMs from 33 patients treated preoperatively with bev-chemo at RM. Graph shows % HGP (replacement, desmoplastic, pushing) scored in each individual lesion and the data are grouped by pathological response score: >75%, 50–75%, 25–49% or <25% viable tumor. Median

number of lesions examined per patient was 1 (range = 1 to 4 lesions per patient). **c–e.** Examples of H&E-stained lesions from the RM cohort are shown. Arrows point to examples of replacement HGP areas. Arrowheads point to examples of desmoplastic HGP areas. Asterisks indicate areas of infarct-like necrosis. **f.** The HGPs and the pathological response to bev-chemo were scored in 128 CRCLMs from 59 patients treated with bev-chemo at MUHC. Graph shows % HGP (replacement, desmoplastic, pushing) scored in each individual lesion and the data are grouped by pathological response score: >75%, 50–75%, 25–49% or <25% viable tumor. Median number of lesions examined per patient was 2 (range = 1 to 12 lesions per patient). The χ^2-test was used to determine statistical significance (see 2 x 2 contingency tables in panels **b** and **f**). Scale bars, 1 mm.

g

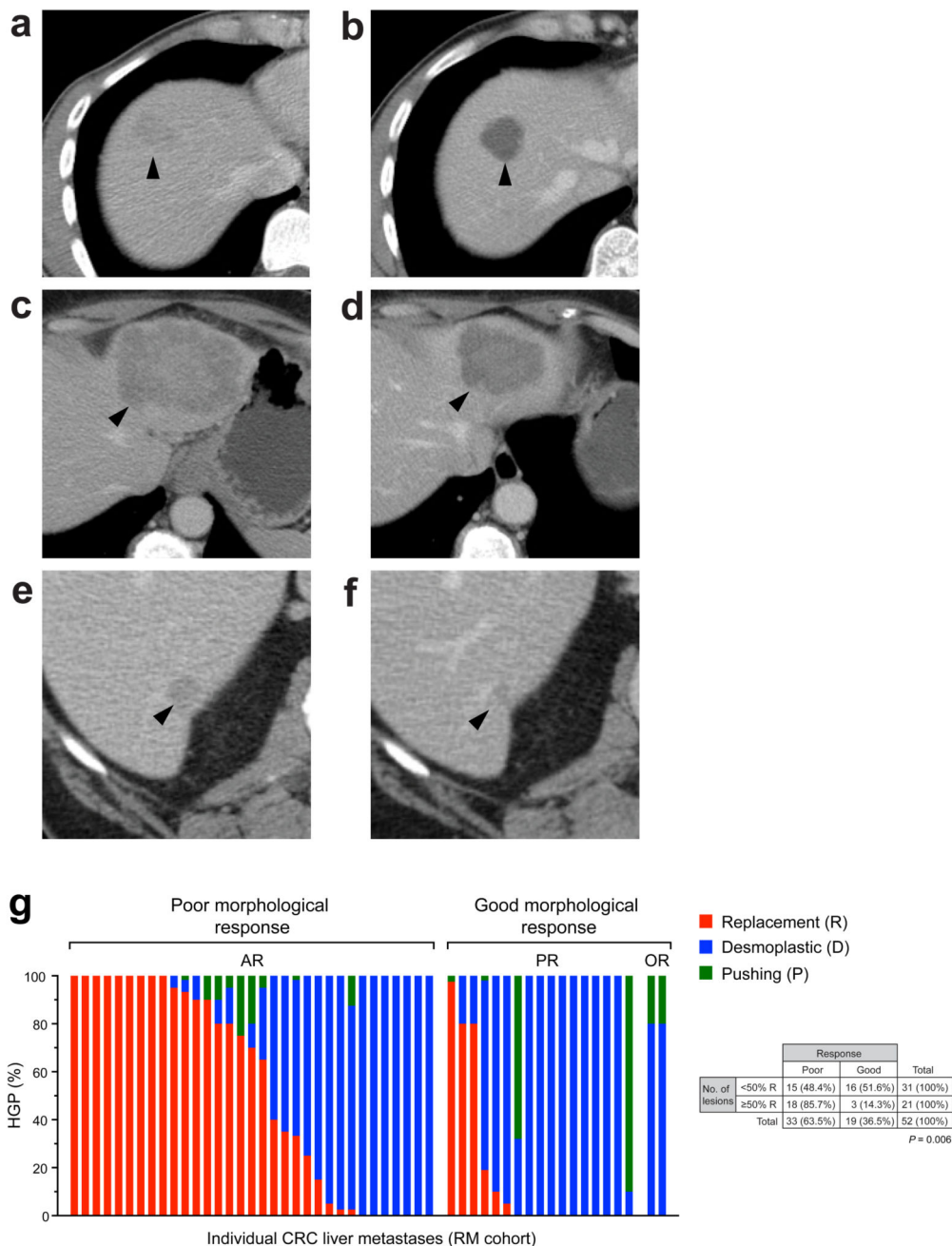|		Response		
		Poor	Good	Total
No. of lesions	<50% R	15 (48.4%)	16 (51.6%)	31 (100%)
	≥50% R	18 (85.7%)	3 (14.3%)	21 (100%)
	Total	33 (63.5%)	19 (36.5%)	52 (100%)

P = 0.006

Figure 2. Correlation between HGP and morphological response on CT in patients treated preoperatively with bevacizumab

a–f. CT scans of patients treated preoperatively with bev-chemo. Examples of optimal (OR), partial (PR) or absent (AR) morphological response are shown.

a,b. OR; in the pre-treatment image a lesion in liver segment VII (arrowhead) is scored as group-3 (**a**); the same lesion imaged after 4 cycles of bevacizumab in combination with CAPOX is now scored as group-1 (**b**).

c,d. PR; in the pre-treatment image a lesion in liver segment II (arrowhead) is scored as group-3 (**c**); the same lesion imaged after 4 cycles of bevacizumab in combination with CAPOX is now scored as group-2 (**d**).

e,f. AR; in the pre-treatment image a lesion in liver segment VI (arrowhead) is scored as group-3 (**e**); the same lesion imaged after 6 cycles of bevacizumab in combination with FOLFIRI is still scored as group-3 (**f**).

g. Morphological response and HGP were scored in 52 liver metastases from 31 patients treated preoperatively with bev-chemo at RM. Graph shows the % HGP scored in each individual lesion (replacement, desmoplastic, pushing). Lesions are grouped according to response: AR, PR or OR. Lesions scored as AR were classed as poor responders, whilst those scored as PR or OR were classed as good responders. Median number of lesions examined per patient was 1 (range = 1 to 4 lesions per patient). The χ^2 test was used to determine statistical significance (see 2 x 2 contingency table in panel **g**).
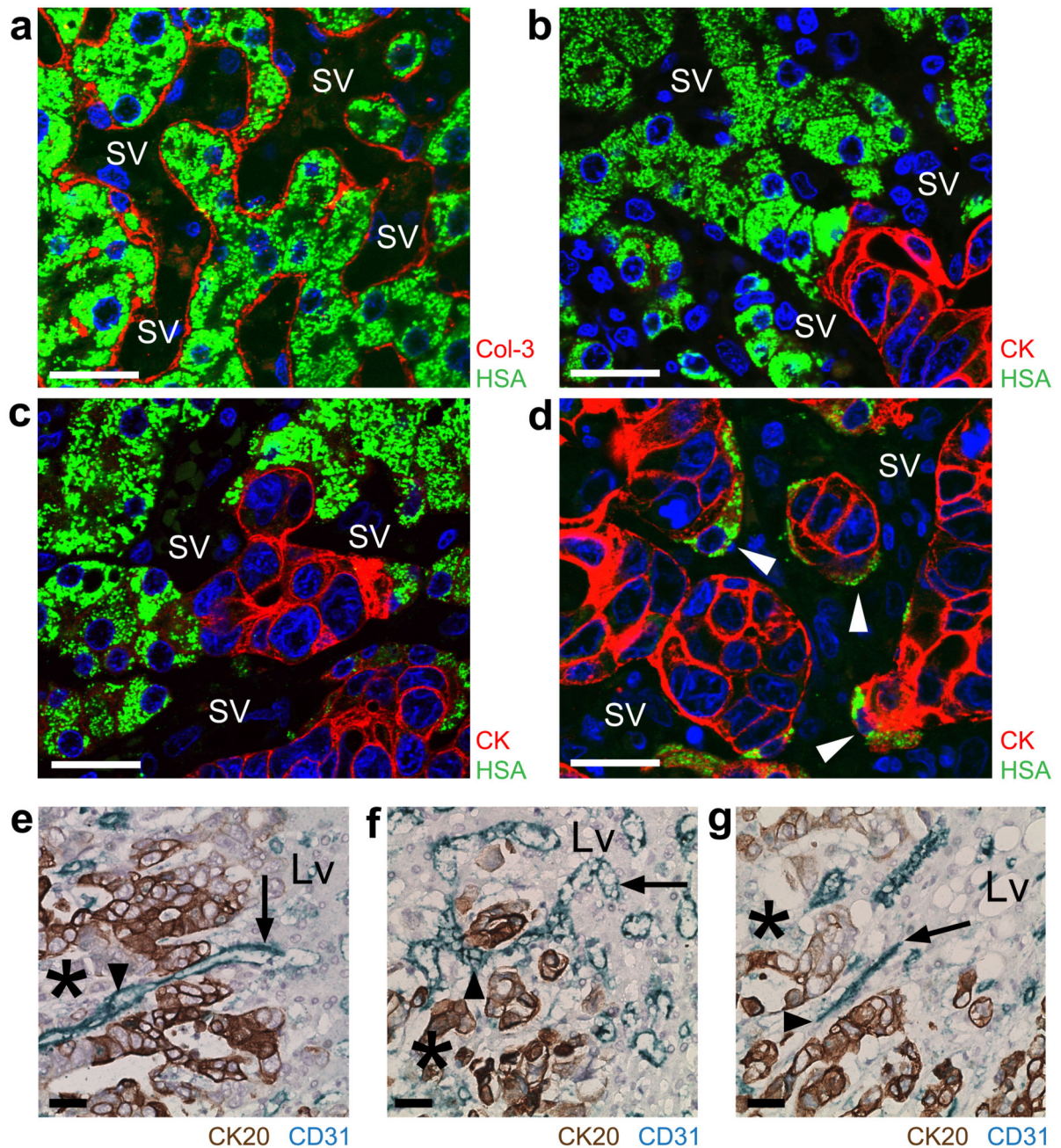
Figure 3. Cancer cells infiltrate the hepatic plates and co-opt sinusoidal blood vessels in the replacement HGP

a. An area of normal liver is shown. Staining is for hepatocyte specific antigen (HSA, green) to detect hepatocytes and collagen-3 (col-3, red) to detect liver sinusoidal blood vessels (SV). **b–d.** Staining for cancer cells (CK, red) and hepatocytes (HSA, green) at the tumor-liver interface (**b,c**) and within the tumor mass (**d**) in a replacement HGP liver metastasis of colorectal cancer. Examples of displaced hepatocytes are marked (arrowheads). **e–g.** Staining for cytokeratin 20 (CK20, brown) to identify cancer cells and CD31 to identify

blood vessels (blue) in replacement HGP liver metastases of colorectal cancer. Arrows and arrowheads indicate examples of liver sinusoidal blood vessels where one end of the vessel is physically located in the liver parenchyma (arrows), whilst the other end is surrounded by cancer cells (arrowheads). Asterisk, tumor. Lv, normal liver. SV, sinusoidal blood vessel. Scale bars, 25 μM.
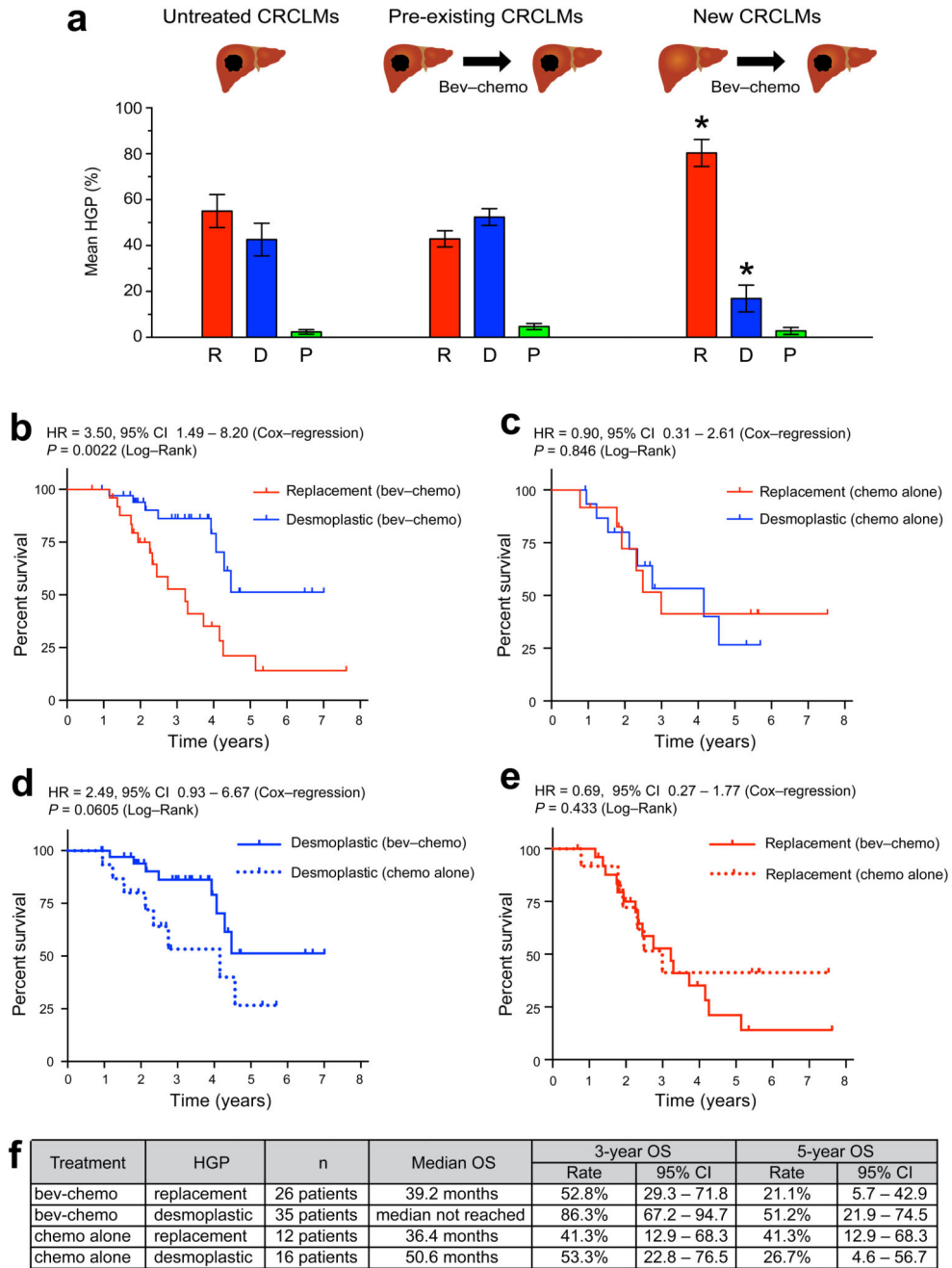
Figure 4. The replacement HGP occurs in progressive disease and is associated with a poor outcome in patients treated with bevacizumab

a. Left: HGPs in untreated CRCLMs (n = 32 lesions from 19 MUHC patients). Middle: HGPs in pre-existing CRCLMs (n = 128 lesions from 59 MUHC patients). Right: HGPs in new CRCLMs (n = 35 lesions from 13 MUHC patients). Graphs show % replacement (R), % desmoplastic (D) and % pushing (P) HGP per lesion ± SEM. **b.** Kaplan-Meier estimates of OS for 62 MUHC patients treated preoperatively with bev-chemo stratified into two groups: predominant replacement HGP (26 patients) or predominant desmoplastic HGP (35

patients). **c.** Kaplan-Meier estimates of OS for 29 MUHC patients treated preoperatively with chemotherapy alone stratified into two groups: predominant replacement HGP (12 patients) or predominant desmoplastic HGP (16 patients). **d.** Kaplan-Meier estimates of OS for 51 MUHC patients with a predominant desmoplastic HGP stratified into two groups: desmoplastic HGP treated with bev-chemo (35 patients) or desmoplastic HGP treated with chemotherapy alone (16 patients). **e.** Kaplan-Meier estimates of OS for 38 MUHC patients with a predominant replacement HGP stratified into two groups: replacement HGP treated with bev-chemo (26 patients) or replacement HGP treated with chemotherapy alone (12 patients). Kruskall-Walls test (**a**) or the Log-Rank test (**b–e**) were used to determine statistical significance. Hazard ratios were calculated using Cox-regression. * P<0.001.
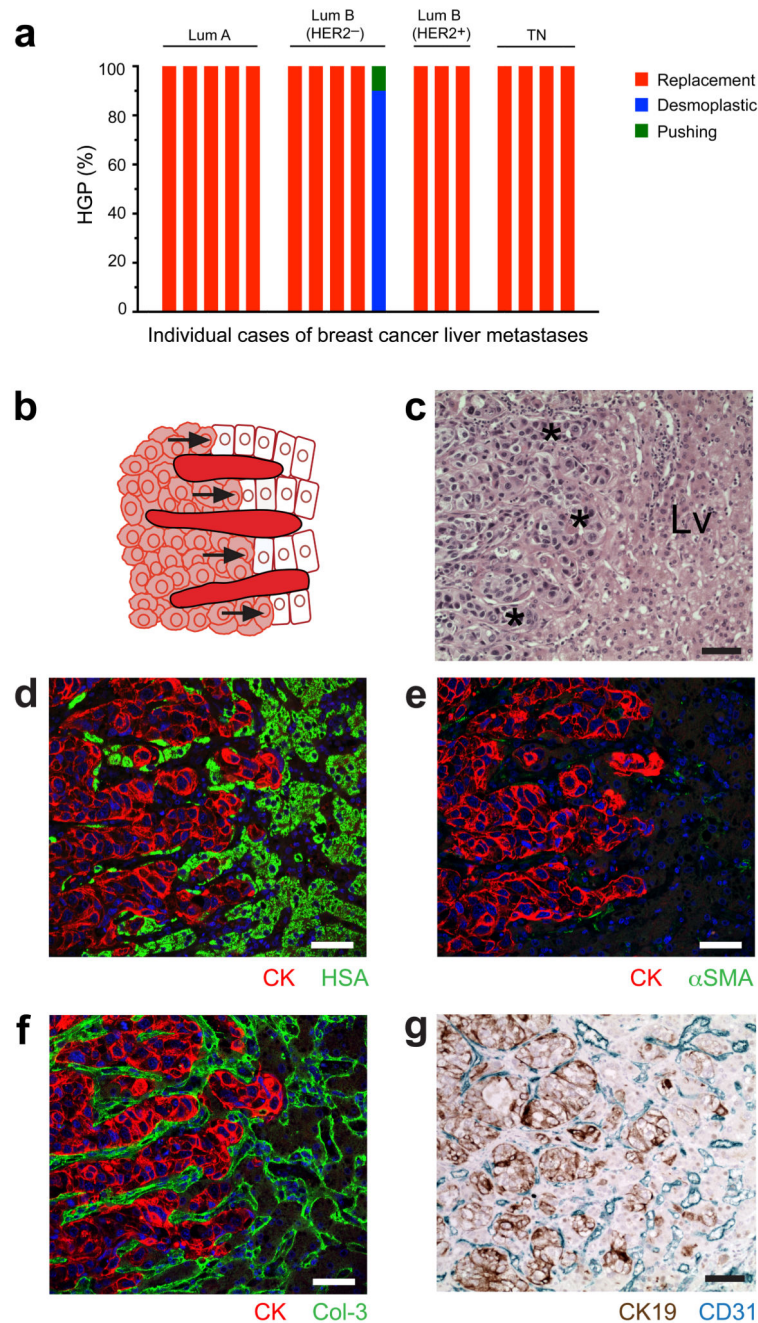
Figure 5. The replacement HGP predominates in breast cancer liver metastases
a. The HGPs were examined in breast cancer liver metastases (BCLMs) from 17 patients. Graph shows the % HGP (replacement, desmoplastic, pushing) scored in each case. The cases are grouped by intrinsic subtype of breast cancer. Lum A, luminal A. Lum B (HER2^{-}), luminal B HER2 negative. Lum B (HER2^{+}), luminal B HER2 positive. TN, triple negative. **b–g.** Morphology of the replacement growth pattern of BCLMs. Diagram of the tumor-liver interface in the replacement HGP (**b**). H&E-stained human BCLM sample illustrating the tumor-liver interface (**c**). Co-staining for hepatocyte specific antigen (HSA) to label

hepatocytes and pan-cytokeratin (CK) to label cancer cells confirms that breast cancer cells infiltrate the liver parenchyma and replace hepatocytes in BCLM (**d**). Co-staining for alpha smooth muscle actin (αSMA) to label fibroblasts and CK to label cancer cells confirms the absence of a desmoplastic stroma at the tumor-liver interface in BCLM (**e**). Co-staining for collagen-3 (col-3) to label sinusoidal vessels and CK to label cancer cells shows that the vascular architecture of the adjacent liver is preserved at the tumor-liver interface in BCLM (**f**). Co-staining for CD31 to label blood vessels and cytokeratin 19 (CK19) to label cancer cells confirms the infiltrative pattern of tumor growth that facilitates vessel co-option in BCLM (**g**). Asterisk, cancer cells; Lv, normal liver. Scale bars, 50 μM.
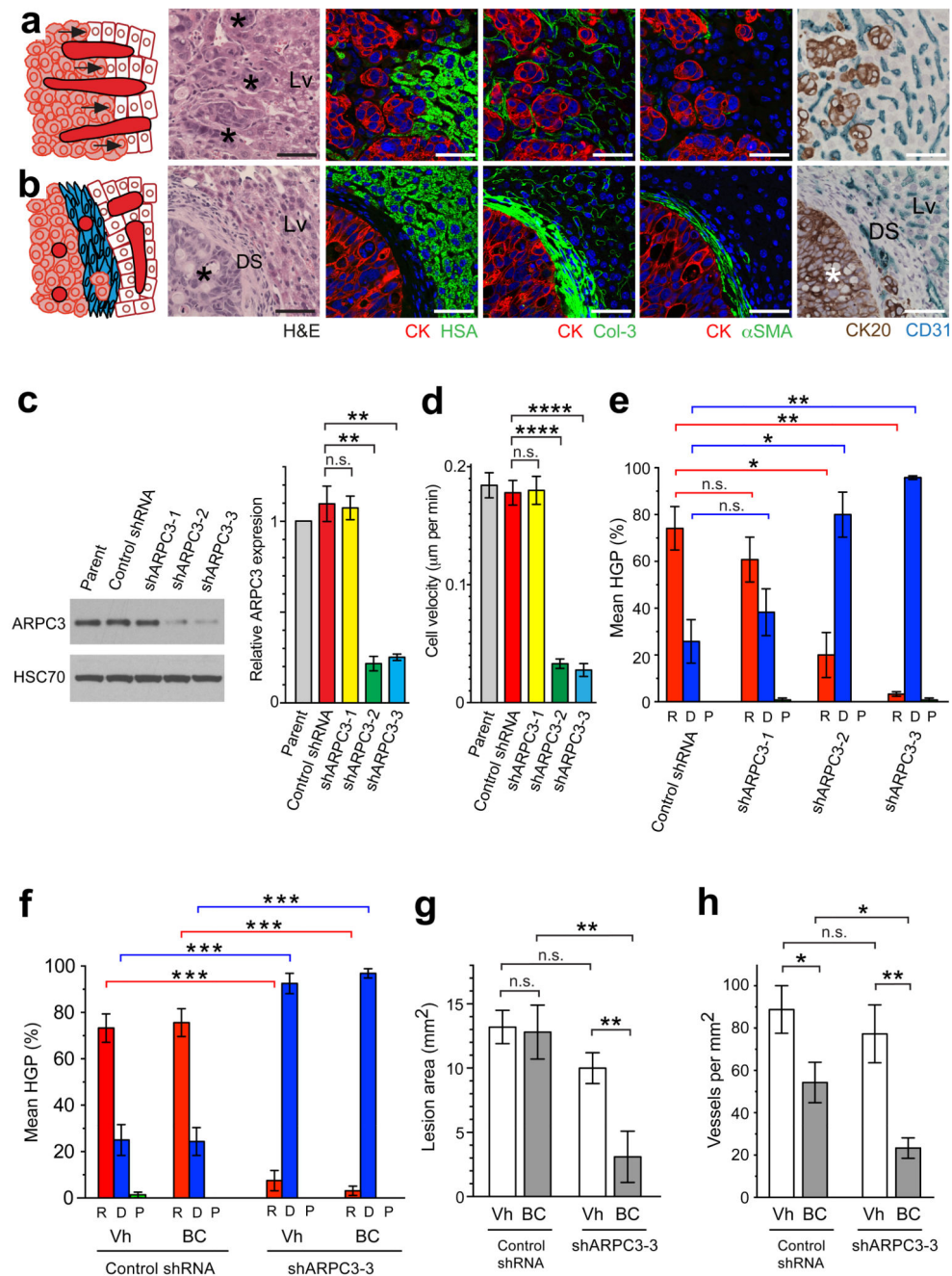
Figure 6. Inhibition of vessel co-option and angiogenesis is more effective than targeting angiogenesis alone

a,b. Areas of replacement (**a**) and desmoplastic (**b**) HGP are shown in a preclinical (HT29 cell line) orthotopic model of advanced liver metastasis. Staining shown is for: H&E, CK and HSA, CK and col-3, CK and αSMA or cytokeratin 20 (CK20) and CD31, as indicated. **c,d.** Characterization of parental HT29 cells (parent) and HT29 cells transduced with control non-targeting shRNA (control shRNA) or ARPC3-targeting shRNAs (shARPC3-1, shARPC3-2 or shARPC3-3). In **c**, ARPC3 expression was determined by western blotting

(see also Supplementary Data Set 1). Graph shows ARPC3 expression relative to parental HT29 cells ± SEM (n = 3 independent western blots). In **d**, cell motility was measured by time-lapse microscopy. Graph shows cell velocity (μm per minute) relative to parental HT29 cells ± SEM (n = 30 tracked cells per group pooled from 2 independent experiments). **e.** Quantification of the HGPs in control- and ARPC3-knockdown tumors. Graph shows the % replacement (R), % desmoplastic (D) and % pushing (P) HGP per group ± SEM (n = 6 mice per group). **f–h.** Tumors with normal ARPC3 levels (control shRNA) or ARPC3 knockdown (shARPC3-3) were established in the livers of mice, followed by treatment with B20-4.1.1 plus capecitabine (BC) or vehicle alone (Vh) for two weeks followed by histopathological analysis. Graph in **f** shows the % HGP per group ± SEM (n = 8 mice per group). Graph in **g** shows liver tumor burden expressed in terms of lesion area ± SEM (n = 8 mice per group). Graph in **h** shows tumor vessel density in terms of vessels per mm^2 ± SEM (n = 8 mice per group). For statistical analysis, Student's t-test (panels **c,g,h**) or Mann Whitney U-test (panels **d,e,f**) were used. *P<0.05, **P<0.01 ***P<0.001, ****P<0.0001. n.s., no significant difference. Asterisk, cancer cells; DS, desmoplastic stroma; Lv, normal liver. Scale bars, 50 μM.